



Fung Institute for
Engineering Leadership
COLLEGE OF ENGINEERING



Increasing Electric Vehicle (EV) Efficiency by Bypassing Regenerative Braking

2nd of May 2022
University of California, Berkeley

GABRIEL Gomes (ME)
MATT ZEBIAK (General Motors)

PATRICK Cheng (ME)
KHOA Nguyen (ME)
VIANNEY GRENEZ (ME)
VICTOR VRAUX (ME)
ANTONIO FLORES (ME)
VICTOR LIN (ME)
RAHUL PATEL (ME)
BRENDAN WHITE (ME)

Academic Year 2021 - 2022

Contents

1 Using alternative methods of coasting in electric vehicles will have lasting industry impacts	3
1.1 Electric vehicles have the potential to change mobility on a global scale	3
1.2 Electric propulsion has less energy consumption and emissions compared to those of an ICE	4
1.2.1 Increasing this efficiency can change the landscape of EV capability, customer base, and environmental impact	4
1.3 Disconnecting axles for the use of coasting may have advantages over regenerative braking systems, and thus improve the vehicle's efficiency and range	4
2 A retrofitted bike tested different scenarios of coasting in a simple manner due to the need for only one motor	5
2.1 Background research shaped the propulsion system requirements	5
2.2 The motor for the system was selected in accordance with a variety of use-case specific factors	5
2.3 Motor specifications guided battery and controller selections	7
2.4 The mechanical drivetrain for the bike system consisted of a custom chain, sprocket, and a mount for the electric motor	8
2.4.1 The desired output speed governed the gear ratio design	8
2.4.2 The drivetrain mounting for the system was assembled using U bolts, washers, and nuts in conjunction with a triangular sheet metal motor mount	9
2.4.3 A disconnecting axle prototype was created for implementing the technology in EVs	12
2.5 The sensor and data collection system consist of an Arduino Mega microcontroller, Secure Digital (SD) card reader, and a variety of sensors.	14
2.5.1 Speed data was acquired using a limit switch	15
2.5.2 Angle data was acquired using an IMU	16
2.5.3 Voltage data acquired through a voltage divider	17
2.5.4 Current data acquired using a current sensor	18
2.5.5 The system outputs data onto SD card for analysis	19
2.5.6 Other general remarks about how the Arduino code is written	19
2.5.7 The implementation of the regenerative braking system	20
2.5.8 Other general remarks about how the Arduino code is written	20
2.6 Testing the prototype in different scenarios and characterizing its attributes	22
2.6.1 How are the losses dependent on the speed ?	22
2.6.2 Linking the theoretical equations to the experimental results	23
2.6.3 Computation of the controller-motor efficiency.	25
2.6.4 The different tests are made based on the energy consumption	28
2.6.5 The limitations of the electric bike approach	29
2.6.6 The testing methodology for data collection follows realistic driving scenarios	31
2.6.7 Study of a daily city commute	33
2.6.8 Impact of the driver behavior on energy consumption	36
3 Conclusion	39
4 Appendix	40

Executive Summary

The electric vehicle (EV) market will likely quadruple by 2030 as consumers continue to invest in EVs to further reduce their environmental impact [1]. What if, with an additional drivetrain component, manufacturers could improve the efficiency and range of EVs? Current EVs use regenerative braking (regen) to recover some energy associated with the vehicles' deceleration; around thirty percent is lost as heat [2]. On the other hand, traditional internal combustion engine (ICE) vehicles coast without regenerative braking when the driver releases the throttle, saving fuel. A disconnecting axle in an EV drivetrain would allow the vehicle to utilize either regenerative braking or traditional deceleration in various driving scenarios, resulting in strategic use of battery power. In partnership with General Motors (GM), our team tested the integration of a disconnecting axle system, which bypasses regenerative braking, to research the axle's potential energy savings.

Our capstone team modeled the disconnecting axle concept with an electric bike and disconnecting wheel hub, which allowed for a faster and more economical study of both the disconnected and connected axle cases. We simulated multiple driving scenarios with this electric bike prototype equipped with an array of sensors, such as a limit switch speed sensor and inertial measurement unit (IMU). By measuring the bike's power usage with the connected and disconnected drivetrain configurations, we demonstrated the promising potential of this technology's impact on EV efficiency. We aspire to transform the current standards for electric drivetrain designs with the disconnecting axle, and therefore revamp EV performance across the industry.

1 Using alternative methods of coasting in electric vehicles will have lasting industry impacts

1.1 Electric vehicles have the potential to change mobility on a global scale

Electric Vehicles (EV) have taken the automotive industry by storm, and are projected to become the future of automotive transportation. The EV market has seen exponential growth from only a few thousand EVs in 2010 to over 315,000 sold annually from 2018 to 2020. During the fourth quarter of 2021, EV sales jumped 72% year over year, as seen in Figure 1 below, indicating the start of mass adoption of electric vehicles. Many of the legacy automakers have pledged to electrify their entire vehicle lineups in the next decade. As automakers transition from gasoline to electric vehicles, many of them are taking their loyal customers with them, which is leading to the rapid growth and adoption of EV's [3].

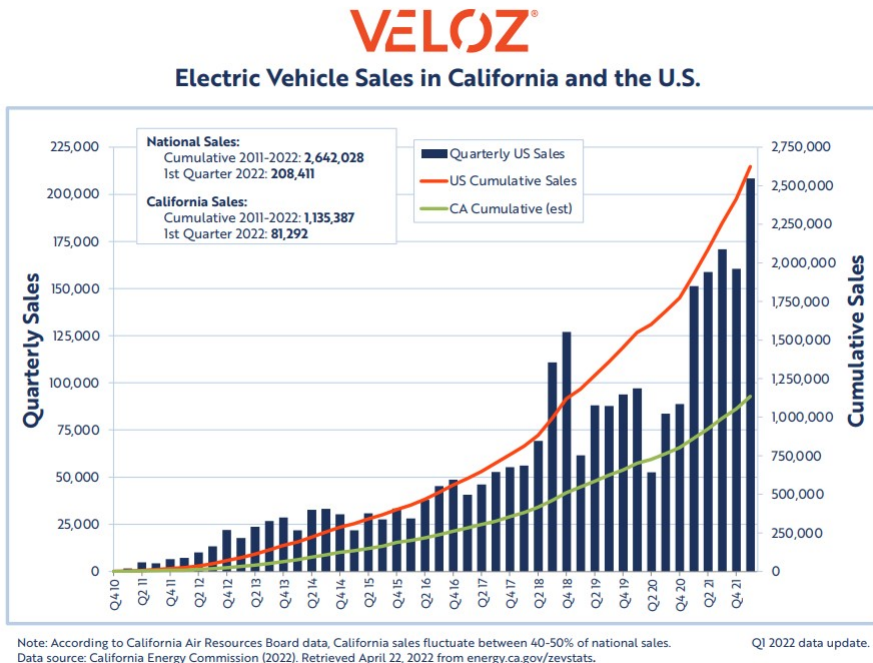


Figure 1: Electric Vehicle Sales in California and the U.S. by Quarter [4]

The electric vehicle market is projected to grow from \$287 billion in 2021 to \$1.3 trillion by 2028 at a compound annual growth rate (CAGR) of 24.3% between the 2021-2028 period. The environmental impact of traditional gasoline vehicles and the exponential increase in fuel prices have pushed consumers towards alternative fuel vehicles on the market [5]. Naturally, many consumers are being pushed towards battery powered and hybrid automobiles that use electric motors as propulsion. Large automakers, such as Tesla, have held a majority of the EV market share for years, and have seen little to no competition, which results in a monopoly of the EV market. Customers that wanted to switch to a battery powered vehicle had very few options aside from a Tesla brand vehicle. However, as more automakers fully electrify their fleets, customers will have a multitude of options when purchasing an electric vehicle. Consumers across the globe now have a transportation method that does not directly harm the environment during daily use.

1.2 Electric propulsion has less energy consumption and emissions compared to those of an ICE

Electric motors are significantly more efficient and environmentally friendly than an ICE. Electric motors can convert over 85% of their electrical energy into mechanical energy, or motion, compared to a gasoline combustion engine, which is only capable of converting up to 40% of the energy contained in its fuel. The inefficiency in an ICE results from the ignition of fuels, such as gas and diesel, that pushes the piston to create motion. Realistically, only 12% to 30% of the energy in gasoline is used to move the vehicle; the rest of the energy is lost as heat. Electric vehicles also have far fewer direct emissions that harm the environment as opposed to gasoline vehicles. Direct emissions exit a vehicle through the tailpipe while driving, during fueling, and also through evaporation from the fuel system. These emissions include nitrogen oxides, greenhouse gases, and various other pollutants that are harmful to the environment and human health. Electric vehicles do not produce direct emissions and have a significantly smaller carbon footprint than gasoline vehicles. Although battery powered vehicles rely on charging from electricity, and some of that electricity is created from coal fired power plants, which are not emission free. Research indicates that carbon dioxide emissions from battery powered vehicles are 40% lower than internal combustion engines. As more power plants are transitioning to renewable energy such as solar and wind, battery powered vehicles will emit less carbon dioxide in the years moving forward [6].

1.2.1 Increasing this efficiency can change the landscape of EV capability, customer base, and environmental impact

Although many automakers and consumers are switching to electric vehicles, a majority of consumers still drive gasoline vehicles and remain skeptical regarding the range and efficiency of electric vehicles. Range poses a particular concern for customers: typical range is currently averaging about 250 miles. However, long range models are being produced with over 300 miles of range. The biggest challenge regarding the range of the EV's are the batteries, which are limited in size [6]. Therefore, we must devise a way to increase the efficiency of EVs while keeping the battery the same. In what follows, we detail how integrating a disconnecting axle system might increase EV efficiency by investigating the effects of the energy usage between current connected axle, regenerative braking EVs and a proposed disconnected axle, no regenerative braking EV.

1.3 Disconnecting axles for the use of coasting may have advantages over regenerative braking systems, and thus improve the vehicle's efficiency and range

Regenerative braking systems provide an overall benefit for EVs because they can recoup a major part of the energy that would normally be lost while driving. However, to optimize the energy use of EVs, bypassing the regenerative braking system is more efficient when the vehicle needs to coast, preserving even more energy in the form of the vehicle's momentum. This energy loss is due to the fact that the regeneration is not 100% efficient, and even power transmission to drive the vehicle is not 100% efficient. Therefore, sacrificing the vehicle's momentum in order to recover some energy, and then accelerate the vehicle back up to speed, may result in an overall loss of energy. This energy loss could be greater than if the vehicle was just allowed to coast and use the momentum of the several-thousand-pound vehicle, then use a small amount of energy to accelerate the vehicle to the desired speed. Of course, the benefit of bypassing regenerative braking is dependent on the driving scenario and what the driver wants their vehicle to do at that moment. Therefore, a system that can accommodate both regenerative braking and coasting is required so energy recovery and usage can be maximized for the highest vehicle efficiency. An electric bicycle with a disconnecting hub can most efficiently study the system due to the minimal cost and simplicity.

2 A retrofitted bike tested different scenarios of coasting in a simple manner due to the need for only one motor

2.1 Background research shaped the propulsion system requirements

The team prototyped an electric bike to model an EV propulsion system for a simpler proof of concept design given time and budget constraints. The first step was to select the bike parts to perform the tests while considering specific design criteria, which are listed in Table 1.

There were several constraints on the motor choice. First, the disconnecting system needed to be easily integrated with the motor. Second, as requested by GM, the motor should be representative of those used in their electric cars. Third, the electrical system had to be safe for the users without high safety requirements. Following electrical equipment safety standards, we limited the working voltage to 40 V DC instead of the maximum 60 V [7]. Finally, to perform the tests, we decided that the bike should be able to attain a speed of 30 km/h on a flat road and at 20 km/h on a 7% slope (which is the maximum allowed slope on highways).

These motor requirements helped curtail battery options. The battery pack had to have a maximum voltage of 40 V and the same nominal voltage as the motor. Additionally, the battery had to withstand the maximum current limit of the motor. Moreover, we required that the battery have sufficient capacity to enable us to conduct tests continuously for one hour while being easily and safely chargeable. Lastly, the motor controller had to be compatible with all of the aforementioned specifications.

Table 1: Propulsion Component Criteria

Motor	Battery	Motor controller
Able to integrate with the disconnecting axle system	Maximum voltage of 40 V	Be compatible with motor ratings
Be a permanent magnet brushless DC (BLDC) motor	Same nominal voltage as motor	Be compatible with battery ratings
Voltage supply lower than 40 V	Capable of handling the motor's maximum current	
Run at 30 km/h on flat roads	Easy and safe charging	
Traverse a 7% slope at 20 km/h	Last for an hour of testing	

2.2 The motor for the system was selected in accordance with a variety of use-case specific factors

Our propulsion system components helped determine the motor's power and torque estimations. To obtain an estimation of this necessary power and torque, we developed a simple algorithm that considered the three main sources of mechanical power losses in a bike: drag losses, friction losses between the wheels and asphalt, and gravitational losses (on inclined surfaces) to compute the minimum required mechanical torque and power that the motor must provide.

The drag losses are computed based on Equation 1 shown below.

$$F_{drag} = \frac{\rho C_d A v^2}{2} \quad (1)$$

where ρ is the density of air, C_d is the drag coefficient of a bike, A is the cross sectional area, and v is the linear speed of the bike. Those parameters were computed based on [8].

The friction losses between the wheels and the ground can be calculated from the normal force of the ground on the wheels multiplied by a rolling friction coefficient, shown in Equation 2. This coefficient is dependent on the surface type and can be found in [8].

$$F_f = \mu mg \sin (\theta) \quad (2)$$

The final force is computed using the gravitational force equation shown in equation 3 shown below.

$$F_g = mg \sin (\theta) \quad (3)$$

where m is the total mass of the bike and the driver, g is the gravitational constant and θ is the angle of the slope. Thanks to this simplified model, we can compute the minimum power required of the motor on both flat ground and a 7% slope:

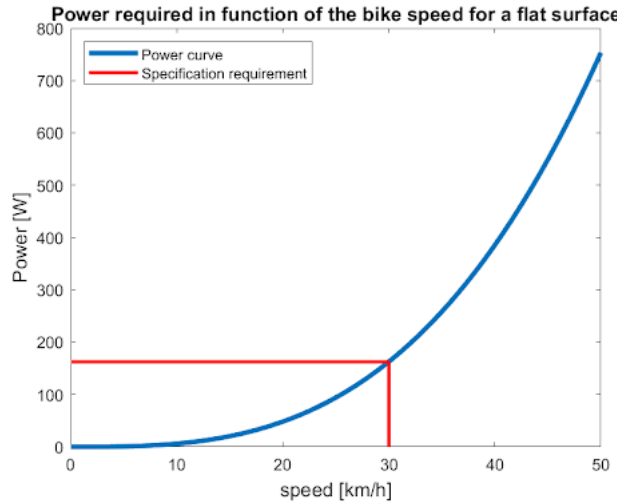


Figure 2: Power expectations on a flat surface

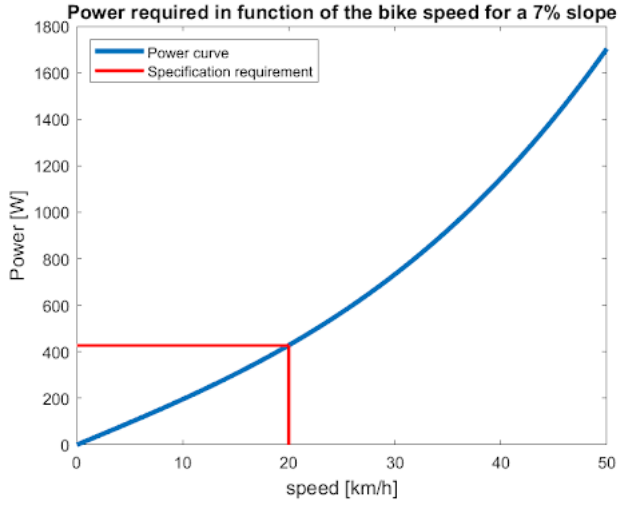


Figure 3: Power expectations on a 7% grade surface

From Figure 2 and Figure 3, we can observe the significant impact of the slope on the power requirements of the bike. In the case of a 7% slope (or in other words, a 4° slope), the necessary motor power is more than doubled. Based on this study and the available motors, we decided to choose a 500 W motor. This choice provides a comfortable margin of 73 W to compensate for the other mechanical losses of the bike.

2.3 Motor specifications guided battery and controller selections

We explored many different options of existing electric bike motors, such as motors that were directly integrated into the bike's wheel and motors that were integrated into the bike's pedal system. Unfortunately, these two systems are not adaptable to our study, as the configurations physically prevent implementation of a disconnecting axle. Therefore, we chose to create a custom design based on a basic 500-Watt permanent magnet BLDC motor.

This decision was between two motors with the same specifications, aside from the nominal voltage: the first was a 24 V motor and the second was 36 V. Initially, a lower voltage can seem more appealing from a safety perspective; however, the second option has two main advantages. A higher voltage means a lower current for the same power rating, and therefore lower energy losses. More importantly, batteries are also commonly manufactured and sold at 36 V; this is due to the main constraint of a battery being its maximal output current. Thus, increasing the voltage decreases the current. We chose a motor with a nominal speed around 2800 RPM (best efficiency) which is much higher than the expected speed of the bike considering the gear ratio. We also expected the motor efficiency to be lower than the manufacturer rating (about 80%).

The battery was selected based on the rated voltage, maximum current, and the required time during which tests could be performed without recharging interruptions (at least one hour). As a result, we chose a 36 V, 15 Ah battery capable of handling 30 A. This 15 Ah battery is able to provide $15 \times 36 = 540$ Wh which serves as an ample buffer for our tests, since full power is not used at all times.

Finally, the constraints on the motor controller were that it had to be working at 36 V, accept a constant current of 20 A as well as current peaks of 25 A, and be compatible with a BLDC motor.

After acquiring the necessary components for the propulsion system, we wired the assembly according to the following schematic shown in Figure 4.

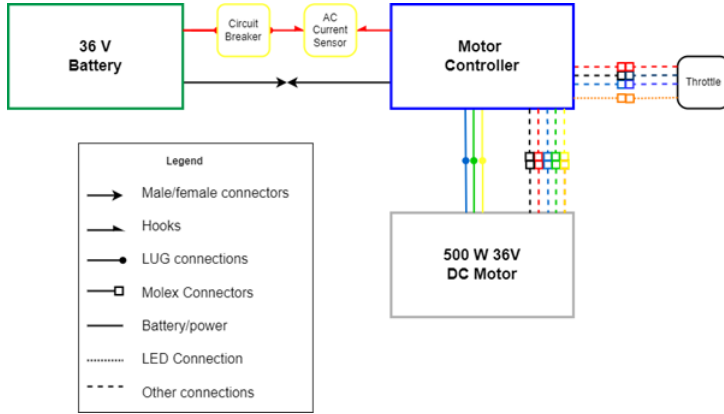


Figure 4: Final electrical schematic

2.4 The mechanical drivetrain for the bike system consisted of a custom chain, sprocket, and a mount for the electric motor

After wiring and testing the necessary propulsion components, we retrofitted the individual components onto the bicycle with a new chain configuration to propel the bicycle forward. The chosen bicycle has a flip-flop hub, where the rear wheel has a fixed gear cog on one side and a freewheel on the other. To change between the two configurations, the wheel must be manually unscrewed and flipped to the desired side, hence a flip-flop hub. The fixed gear cog side simulated the connected axle case since the wheel turns the motor when coasting. In contrast, when the chain was connected to the freewheel side, the wheel would be able to spin freely without turning the motor and resembled a disconnected axle in coasting.

2.4.1 The desired output speed governed the gear ratio design

When designing the chain and mounting configuration, a sprocket was added to the rear wheel to help us reach a maximum velocity of 40 kph (24.85 mph). The number of teeth on the sprocket was calculated with the desired velocity in consideration. A required output of 203 revolutions per minute (RPM) was computed using our wheel radius of 0.33 m.

Furthermore, we obtained the number of teeth needed on the rear wheel through Equation 4, also shown below, where RPM_{in} is the motor's angular velocity, and S_{motor} is the number of teeth on the motor's output gear. Our motor has the capacity to run at a maximum speed of 3000 RPM, however calculations were determined assuming a speed of 1500 RPM thus running the motor at 50%. Taking into consideration all these factors, a 54-tooth sprocket met the requirements thus resulting in a 4.95 gear ratio.

$$S_{rear} = \frac{RPM_{in}}{RPM_{out}} S_{motor} \quad (4)$$



Figure 5: 54-Tooth Rear Wheel Sprocket

The sprocket, Figure 5, was chosen to have 54 teeth and more importantly, to fasten onto the existing sprockets of the rear wheel. Since the motor would not be able to be placed in the same location as the bike pedals, a new location would have to be determined, thus requiring a new chain configuration to connect the 11-tooth motor output to the 54-tooth sprocket at the rear wheel. Next, the team worked towards mounting and aligning all components onto the bicycle to assemble a working drivetrain that could be used to test different coasting scenarios.

2.4.2 The drivetrain mounting for the system was assembled using U bolts, washers, and nuts in conjunction with a triangular sheet metal motor mount

The drivetrain mounting solution had a few requirements: being mounted on two diverging chassis tubes, having slots for position adjustments, producing enough counter torque against the motor, and finally, supporting the motor's weight.

To accomplish a successful motor mounting, the team initially attempted bolting the motor directly to the frame, as seen in Figure 6, using u-bolts, rated for over 1000 lbs. This method of motor attachment was possibly the most secure option, but suffered from a misalignment issue; due to the positioning of the motor, the output gear of the motor (sprocket) was positioned too far away from the wheel sprocket, laterally. The amount of lateral chain flex and movement required would have induced severe inefficiencies. Additionally, the chain would have interfered with the frame of the rear triangle, and most likely would not have stayed on either sprocket.



Figure 6: Motor Mounting Schematic on Bike Frame

The mounting solution for the bike system was initially intended to position the motor in the rear triangle of the bicycle frame, as seen in Figure 7. Unfortunately, the mass and shape of the motor makes mounting at this location very difficult due to bending moments exerted on any potential mounting solution. The solution to this issue was to mount the motor in the central triangle of the bicycle frame, above the bottom bracket. Then, we extended and routed the chain around the arm of the rear triangle, similar to the chain routing of a regular bicycle chain, as shown in Figure 8.

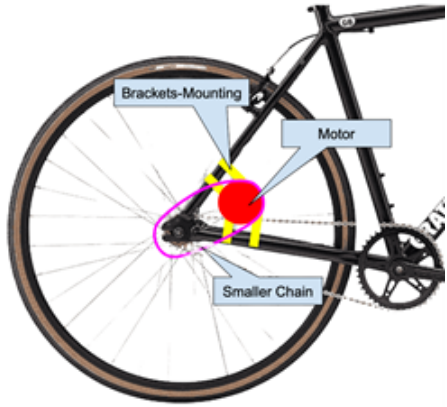


Figure 7: Initial Motor Mounting Schematic on Rear Triangle



Figure 8: Chain Routing from Motor to Rear Wheel

A sheet metal triangle, bent to align with the front triangle of the bicycle frame tubes proved most effective. The top segment of the triangle served as a flat plate for the motor to rest on, and included slots for adjustment. U-bolts mounted the bracket to the frame, as they provided a superior clamping force onto curved objects like the tubes of the frame. Lock washers provided additional clamping force, and reduced any loosening due to vibration. The last detail was the inclusion of washers in addition to the u-bolt plates. Increasing the surface area of the clamp reduced stress concentrations in the sheet metal making up the mount, and distributed the clamping force generated by the nuts and bolts in the mounting solution. Although the mounting solution is effective, there are also some limitations. The support is not completely rigid and the high position of the motor in relation to the bike frame makes the alignment of the chain also uncertain. The final design is shown below in Figure 9 with the motor unattached and attached.

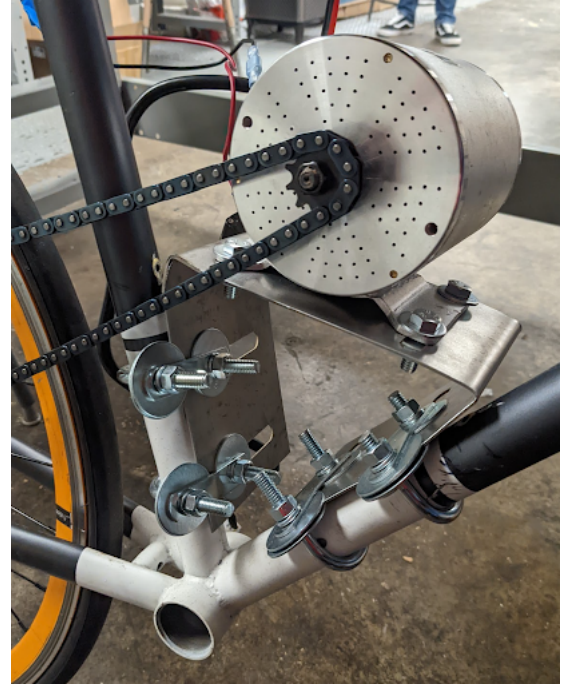


Figure 9: Mounting Bracket Attachment Details

2.4.3 A disconnecting axle prototype was created for implementing the technology in EVs

In order to visualize what a disconnecting axle would look like in an automotive application, the mechanical team designed a prototype of a potential disconnecting mechanism. The figures below show a tabletop display of a disconnecting axle, which is heavily inspired by a manual transmission found in modern vehicles.

The handle, which represents the vehicle's electric motor, can be turned by hand to provide an input rotation to the system. The handle is connected to the shaft and drive gear. The handle, shaft, and drive gear always spin at the same angular velocity. The drive gear then engages with the collar, which also spins at the same speed as the drive gear. The collar can slide axially (left and right) along the drive gear by input from the shift fork, and engage with the output gear when needed. As shown in Figure 10, the collar is not engaged with the output gear. This position of the collar allows the output gear, which represents the wheel of the car, to spin freely and independently from the handle, or motor. This case is the disconnected position of the mechanism. For the connected axle position, the collar slides to engage with the output gear and transmits the rotation it's receiving from the handle, or motor. As a result, the output gear, which would be connected to the wheel of the car, spins at the same speed as the input, as Figure 11 shows.

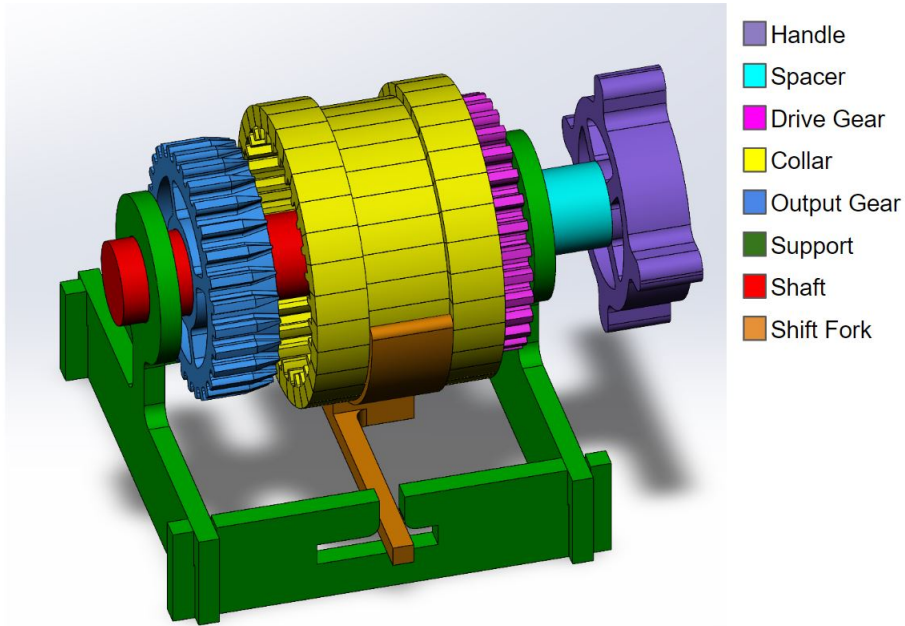


Figure 10: Disconnected Position

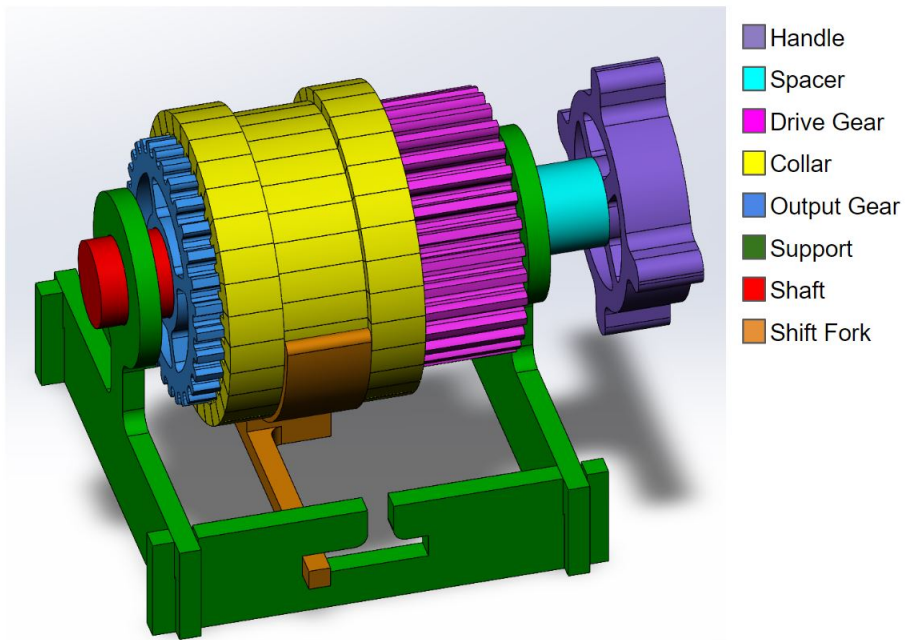


Figure 11: Connected Position

2.5 The sensor and data collection system consist of an Arduino Mega microcontroller, Secure Digital (SD) card reader, and a variety of sensors.

The data acquisition (DAQ) system employed a suite of electronics. The sensors consist of a gyroscope, accelerometer, voltage sensor, current sensor, and limit switch which measure angular velocity, acceleration, voltage, current, and speed, respectively. The microcontroller used is the Arduino Mega, which writes the output data onto a micro SD card for further analysis. The DAQ system schematic is detailed below:

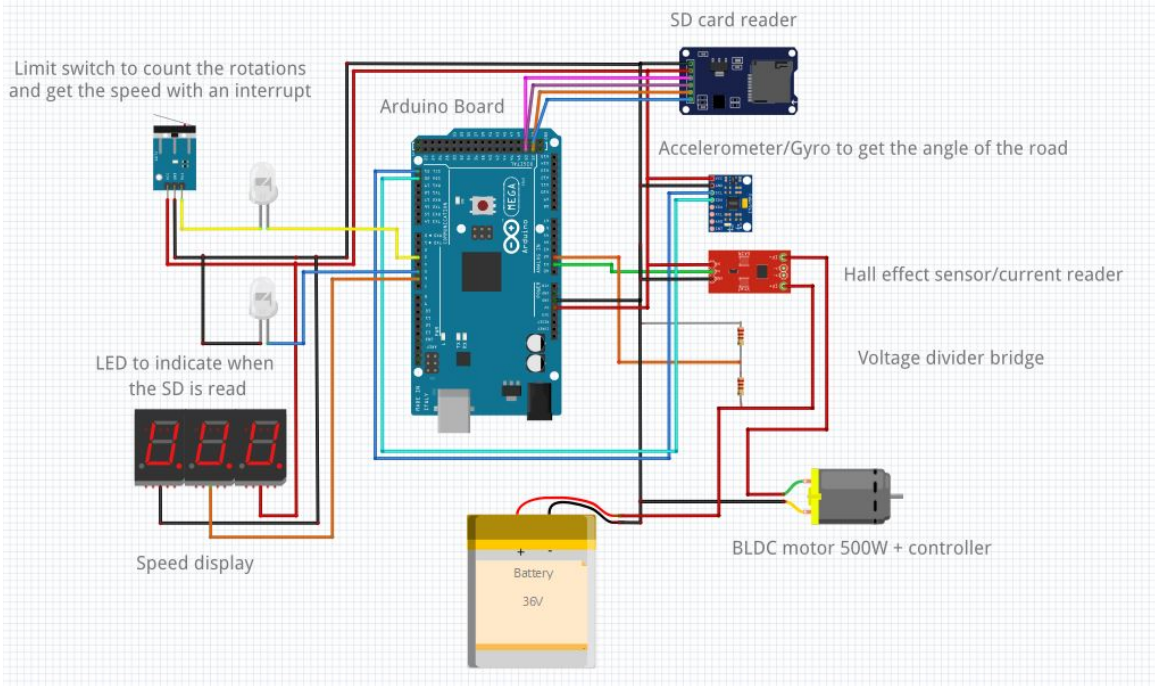


Figure 12: Main data acquisition circuit

In terms of controls, two servo motors allow regen simulation by applying partial braking pressure while coasting. This mechanism simulates the quick deceleration felt in EVs when the driver releases the throttle and regenerative braking occurs. By comparing the non-regen and regen trials, we will make a recommendation to GM of whether coasting is a viable EV feature.

Before digging into each sensor and how they are used, here is an image of the whole bike, with the mechanical parts, the electrical parts and the sensors.



Figure 13: Our prototype

2.5.1 Speed data was acquired using a limit switch

Bike speed is an important factor in determining the energy expenditure of the bike as it provides a measurement of the outputted mechanical energy while driving. To obtain the bike speed, we attached a limit switch sensor to the front fork of the bike. The switch tracks speed by registering a full revolution of the wheel every 8 pulses triggered by the wheel spokes. We were aware that this sensor could create problems during testing and would be easily damaged; however, after having tried available optical and magnetic sensors for an Arduino, we observed that the limit switch was the only sensor able to handle high rotation speeds.

The limit switch's wiring to the Arduino can be seen in Figure 13. The limit switch sensor is wired to the analog pin of the Arduino in order to acquire time data. Using this data, we can calculate the amount of pulses

per revolution of the wheel. Following this, the RPM of the bike wheels can be calculated using Equation 5 shown below, where pulses are the amount of times the limit switch sensor is contacted by the spokes in the given time frame, and t is the time frame or change in time in milliseconds. The Arduino code associated with the speed data collection can be found in [9].

$$RPM = \frac{\text{pulse}}{2\text{pulses per revolution} \Delta t} \frac{1000 \text{ ms}}{1 \text{ sec}} \frac{60 \text{ sec}}{1 \text{ min}} \quad (5)$$

Multitasking is an interesting aspect of the speed DAQ code [9]. The Arduino does not handle multitasking well, although multitasking is not specifically required for our project because we are only collecting data. The code utilizes interrupts, which are common features of micro-processors in general, as these functions constantly work in the background of the code. An interrupt is a method that calls a function as soon as a change is detected in the corresponding pin. Contrary to any method used in the void loop, an interrupt becomes an immediate priority as soon as it is triggered. A trigger can be, for instance, a change from a low signal to a high signal.

In our configuration, the limit switch is associated to the interrupt and is triggered as soon as a wheel spoke activates the switch. The called function simply increments a counter. In our case, we used an interrupt because we need to constantly count the spokes for subsequent calculations. Interrupts enable this simultaneous speed data collection while the main void loop is running, preventing any time conflict priority in the code.

To verify the accuracy of the RPM data, a tachometer, a device used to read the angular velocity of rotating objects, was used to measure the rpm of the wheel. After comparing the RPM data collected by both the Arduino and the tachometer, the former was deemed accurate and reliable, thus enabling use of the limit switch mechanism.

The wheel's dimensions and rpm allowed us to calculate the bike speed. This calculation is done in the MATLAB code [10]. The equation associated with calculating the bike speed can be found in Equation 6 below, where r , the radius of the bike wheel, was measured to be 0.33 meters using a tape measure:

$$v = RPM \frac{1 \text{ min}}{60 \text{ sec}} \frac{2\pi r \text{ meters}}{1 \text{ revolution}} \frac{3.6 \text{ km/h}}{1 \text{ m/s}} \quad (6)$$

2.5.2 Angle data was acquired using an IMU

The measurement of the road angle is important because this parameter has a direct impact on the torque that the bike has to provide. By knowing the evolution of this angle through the vehicle's path, the required mechanical power at each moment can be calculated.

To measure the angle of the road, we use an accelerometer (on-board) and gyroscope (MPU-6050). These sensors are sensitive to the variation of acceleration in the Z-axis (perpendicular to the bike's movement) and to the angle in the Z-axis. The wiring associated with these sensors can be seen in Figure 14.

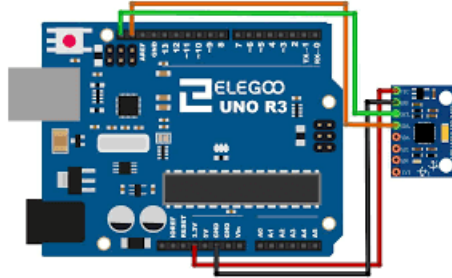


Figure 14: Angle Acquisition

The accelerometer and gyroscope data are prone to systematic errors. The accelerometer provides accurate data over the long term, but is noisy in the short term. The gyroscope provides accurate data about changing orientation in the short term, but the necessary integration causes the results to drift over longer time scales. According to [11], combining the accelerometer and gyroscope data resolves this issue because the errors cancel out. These two inputs are commonly combined with a Kalman Filter, which is quite complex. Fortunately, these two data types can be combined with a simpler approximation, called a Complementary Filter. The approximate formula to combine the accelerometer and gyroscope data is shown below in Equation 7.

$$\text{Filtered Angle} = \alpha(\text{Gyroscope Angle}) + (1 - \alpha) \times (\text{Accelerometer Angle}) \quad (7)$$

where: $\alpha = \frac{\tau}{(\tau + \Delta t)}$ and (Gyroscope Angle) = (Last Measured Filtered Angle) + $\omega\Delta t$. Δt is the sampling rate, τ is the time constant greater than the timescale of typical accelerometer noise. The product of these modifications were determined to be an accurate and reliable measure of the angle through testing with a second party angle measurement application.

2.5.3 Voltage data acquired through a voltage divider

The voltage outputted by the battery is crucial in determining the battery power output during testing to determine energy expenditure. Therefore voltage data was required during testing of our prototype.

The Arduino's ability to read voltages enabled data collection of our battery's voltage. The wiring from the battery to the Arduino can be seen in Figure 13 and is wired to the analog portion of the Arduino to obtain continuous time data. Because the Arduino can only read voltages up to 5V and the battery used is a 36V battery, a voltage divider, which can be seen in Figure 15, was connected to the battery and motor controller in parallel and the output voltage was wired to the Arduino.

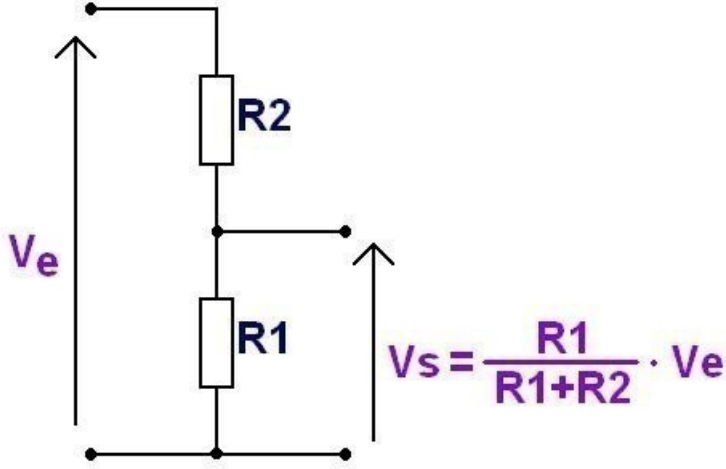


Figure 15: Voltage Divider Bridge

The divider divides the voltage from the battery by 10 kOhms; with $R1$ being 1 kOhm, and a 5kOhm, and two 2 kOhm resistors in series to make 9 kOhms as $R2$, seen in Figure 15. The divider is used in order to obtain a readable value for the Arduino. As the Arduino reads the voltage data in bits, instead of the desired unit of volts, the Arduino code associated with the voltage readings converts the bits of voltage read by the Arduino into readable voltage values which can be found in the GitHub link. The code also accounts for the offset voltage taken, and averaging over multiple values to obtain accurate readings. The equation used to calculate readable voltage values can be found in Equation 8 shown below.

$$V_{real} = \frac{50 \text{ V}}{1025 \text{ Bits}} V_{read} \quad (8)$$

In order to verify the accuracy of the voltage data, a digital multimeter, a device used to read voltages, was connected to the battery and motor controller in parallel. The readings from the digital multimeter confirmed that the Arduino collected reliable and accurate voltage data.

2.5.4 Current data acquired using a current sensor

Similar to voltage data, current data is also required when determining the power outputted by our battery, which determines energy expenditure. An ACS712 current clamp, connected from the battery to the motor controller in series and to the analog portion of the Arduino, collects continuous time current data. The connections associated with the current clamp can be seen in Figure 13. The current clamp collects current data through the hall effect, where the current read from the clamp is used to send a voltage reading to the Arduino.

To verify the accuracy of the current data by the Arduino, a digital multimeter used as an ammeter, a device used to accurately read current, was connected in series with the battery, motor controller, and the current clamp. From the current readings outputted in the Arduino integrated development environment (IDE) and the readings from the digital multimeter, it was evident that the current clamps readings were inaccurate; however, the readings could be correlated to the real values. Therefore, multiple readings were taken from the digital multimeter and from the current clamp to interpolate a function that would be used in the Arduino code to output the correct current readings [9]. The code again accounts for this function, as well as for an

offset of the current value readings, seen in Equation 9 shown below, and is averaged over multiple values in order to obtain accurate current readings.

$$I_{real} = I_{read} - I_{offset} \quad (9)$$

2.5.5 The system outputs data onto SD card for analysis

In order to collect and analyze the data, the Arduino outputs the data it collects from the sensors into a text file inside the SD card connected to the SD card reader. The SD card reader's wiring to the Arduino can be seen in Figure 13, and the associated Arduino code to output the data into a text file can be found in the GitHub link [12].

Once a trial for testing is complete, the SD card can be removed from the SD card reader, placed into a USB adapter, and accessed using a laptop or computer. Using the Matlab code found in the GitHub link [10], the text file of the collected data inside the SD card can then be plotted and later analyzed. In Figure 17, we can see an example of the final output of the code. Each result of our tests will be based on the analysis of graphs like these.

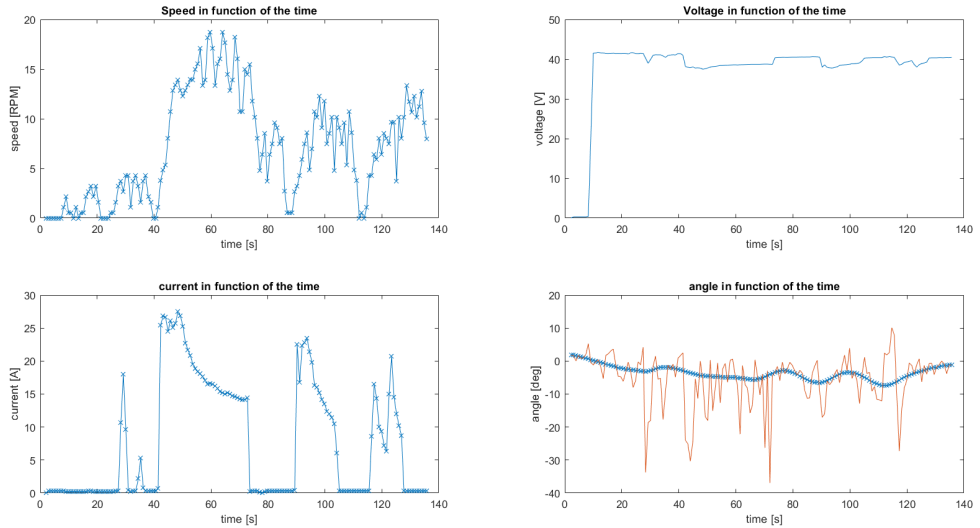


Figure 16: Example of an output of one test, using Matlab to plot the data gathered by the Arduino chip

2.5.6 Other general remarks about how the Arduino code is written

A big issue when it comes to programming an Arduino is to make the loop as fast as possible. A happy medium has to be found between the accuracy of the data points and the time to obtain them. For instance, to get a precise and accurate value of the current, we wrote a smaller loop inside the void loop to average the input data. It is an easy way to filter any outliers and smooth the data acquisition. On the other hand, this small loop takes time to run, and during this period the code is only focused on the current, and ignores the data of the other sensors, as the Arduino is not multi-tasking. This is why all of the sensor loops must be as fast as possible. By checking the final results and comparing it to actual measurement devices such as tachometers or multi-meters, we determined an optimal number of loops for each sensor, depending on the quality of the sensor and the fluctuation of the data.

For the same reason, we decided to write one time on the SD card instead of after each data acquisition because the process of writing on an SD card takes a few milliseconds, which is relatively long compared to other actions, and it is beneficial to reduce it as much as possible. In opening the SD card file 5 times for speed, angle, voltage, current, and time in the void loop, we modified our code to have only one writing of all the data. This allows us to ensure that all the data points are taken almost at the same time and that there is no delay between readings.

2.5.7 The implementation of the regenerative braking system

The purpose of the project is to compare the energy efficiency of an EV in two cases :

- The classic case: the vehicle has regenerative braking and a connected axle
- The new concept: No regenerative braking, but a disconnected axle

In the first case, the main aspect is that the battery is charged as soon as the vehicle is slowing down. In this case, the motor is used as a generator to provide some energy back to the battery. It is particularly efficient when the car needs to slow down because the energy that is usually lost in the brakes due to friction is not wasted (though partially recovered) and charges the battery. The downside of this technology is that the regenerative braking system strongly decelerates the car by approximately 0.1 g in GM vehicles.

Implementing a disconnected axle creates an alternative to regen. In this case, when the vehicle is coasting and has no positive acceleration, the motor and the wheels are disconnected and most of the friction losses of the drivetrain, in addition to some motor internal losses, are eliminated. In the case of GM, the permanent magnet BLDC motors are experiencing iron and Eddy current losses even when no current is flowing. This could lead to situations where coasting saves more energy than using the regenerative braking system. The purpose of this research is to determine efficient driving scenarios for a disconnected axle system, and advise GM on the viability of further researching this new concept.



Figure 17: Our physical implementation of the Regenerative braking simulation

2.5.8 Other general remarks about how the Arduino code is written

To run our tests and more accurately compare the two cases, we must consider the deceleration of 0.1 g in the vehicle, otherwise our comparison would be biased. The issue with our prototype is that the battery cannot bear a positive input of current of more than 3 A. To address this, we have implemented a system that enables us to simulate the braking effect and to compute the theoretical energy savings.

We implemented two servo motors, controlled by an Arduino board, which actuate the bike's brakes to create

the corresponding deceleration. We can see this additional circuit in Figure 18. The Arduino receives the input of the throttle and recognizes when the motor is on. As soon as the throttle is released, the servomotors engage the brake pads. The servomotors are mounted onto the bike with a custom 3D-printed mount.

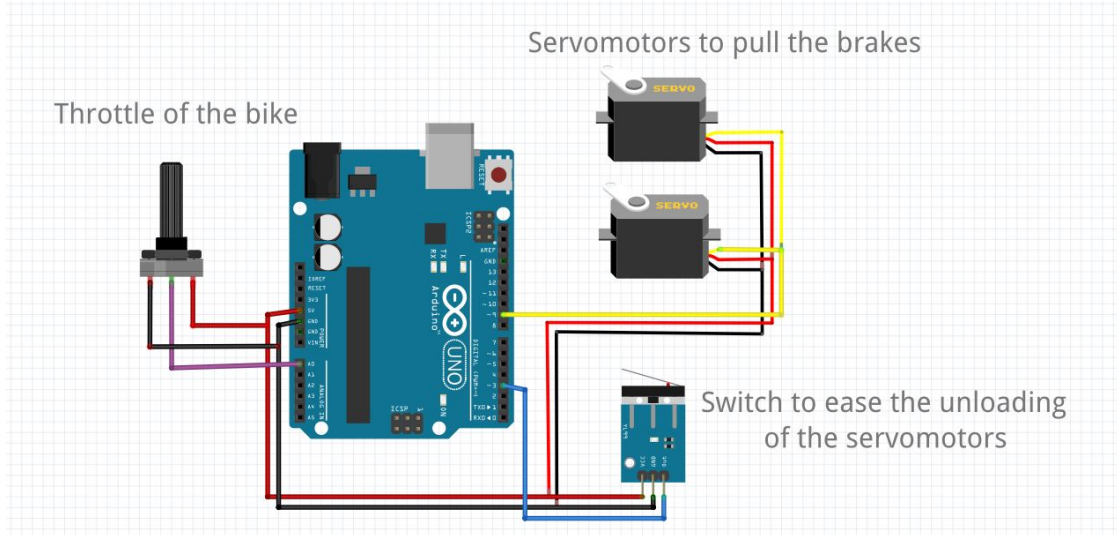


Figure 18: Circuit to control the brakes and simulate regen's impact on acceleration

By comparing the evolution of the speed with and without the servomotors, we have been able to adjust the braking force to correspond to a deceleration of 0.1 g. We achieved this value by tuning the pressure of the bike's front brakes.

In Figure 19, we can see that the difference between the slope of these two curves, which we approximate as being lines, is equal to 0.1 g and representative of GM vehicles.

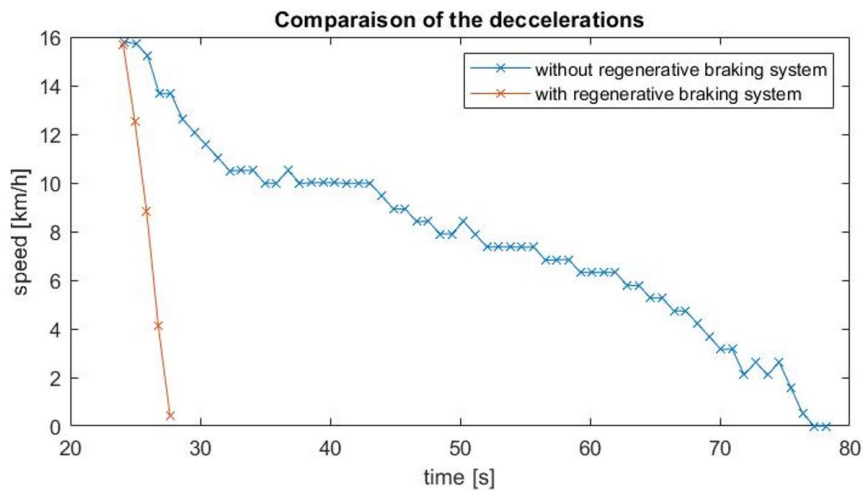


Figure 19: Evolution of the speed with and without regen

2.6 Testing the prototype in different scenarios and characterizing its attributes

2.6.1 How are the losses dependent on the speed ?

Prior to beginning tests, it is important to characterize the energy losses of the bike. First, it is required to observe the difference in loss distribution between the losses of a car and of the prototype. Second, it provides a consistent and scientific way to isolate the losses due to the regenerative braking system and to set them to provide a deceleration of 0.1 g. Finally, it gives an idea of the overall efficiency of the bike.

To compute the loss distribution, three different cases had to be studied: the disconnected axle case, the connected axle without the regenerative braking system and finally, the case of the connected axle with the regenerative braking system.

Disconnected axle

In this case, the motor is disconnected from the wheel when the wheel is spinning faster than the motor. Therefore the mechanical power losses when the wheel is spinning faster are due to:

1. The drag due to air resistance (eq. 1)
2. The friction losses between the tires and the ground (eq. 2)
3. The gravitational force (eq. 3)
4. The losses in the wheel bearings¹

Connected axle without regeneration

In this configuration, the motor is always connected to the wheel. Therefore, it mimics the losses occurring in the disconnected case when the motor is providing power to the bike, but also the losses consistently occurring in the connected axle scenario. This leads to new losses in addition to those above:

1. Friction losses due to the chain. Based on [13], these losses can be modeled as $P_{chain} = C_1v$
2. The losses occurring in a motor with the phases in open circuit. Such losses have multiple sources: ball bearing losses, eddy current losses, and iron losses, which lead to power losses depending on the speed [14]. Therefore, they can be modeled using Equation 10 below.

$$P_{motor} = C_1v + C_2v^2 \quad (10)$$

Connected axle with regeneration

In this final case, the losses from the previous case are present but on top of that, when the bike is decelerating, an additional 'loss' is created. In this case, the motor is used as a generator to provide energy back to the motor. GM, like many other manufacturers, decided to implement the controller so that the deceleration due to this regeneration is a constant 0.1 g [m/s^2]. Therefore, we have implemented the automatic braking system to simulate that effect and require the power loss shown in Equation 11 below.

$$P_{regen} = Fv = (m \frac{dv}{dt})v = (m0.1g)v \quad (11)$$

¹where the power losses have a part proportional to the speed and a part proportional to the square of the speed: $P_{bearings} = C_1\omega + C_2\omega^2$.

where F is the force applied on the bike due to the regenerative braking system, m is the mass of the bike and the driver, and v is the linear speed of the bike.

2.6.2 Linking the theoretical equations to the experimental results

To compute the losses in the different cases and efficiency of the bike, we have decided to use the method presented in [15], with modifications for our bike. The method consists of measuring the bike's speed over time during deceleration on a flat surface. This kind of experiment provides a curve as seen in Figure 20. Based on that test, Newton's second law gives the total losses of the bike at every moment shown in Equations 12 and 13 below.

$$m \frac{dv}{dt} = F_{motor} - F_{losses} \quad (12)$$

$$m \frac{dv}{dt} = -F_{losses} \quad (13)$$

where m is the mass of the bike and the driver, v is the linear speed of the bike, F_{motor} is the force provided by the motor on the bike (equal to zero when the motor is off) and F_{losses} is the force created by the sum of all the losses cited before. This relation allows to compute the power losses in function of the speed shown in Equation 14 below.

$$P_{losses} = -m \frac{dv}{dt} v \quad (14)$$

Based on this method and several deceleration tests (see Figure 20 for an example of deceleration with the axle connected and the regeneration system deactivated), we were able to fit the power losses for each case with a third order approximation of the form shown in Equation 15.

$$P_{losses} = C_1 v^3 + C_2 v^2 + C_3 v \quad (15)$$

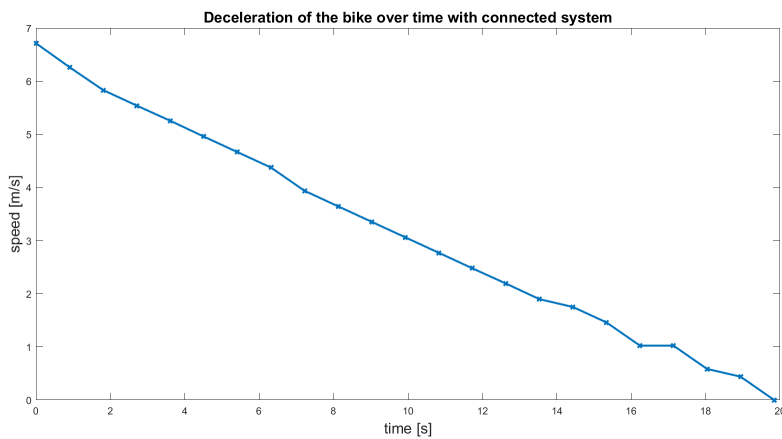


Figure 20: Deceleration with connected axle

These tests provided the parameters of Equation 16 (disconnected axle) and of Equation 17 (connected axle). This second equation represents the mechanical losses that the bike has to overcome to ride at constant speed in both cases. In both situations, the motor and the wheel are spinning at the same speed and therefore the wheel is considered connected to the motor. The plot of those results can be found on Figure 21.

$$P_{\text{disconnected}}(v) = -0.02285v^3 + 2.41v^2 + 1.098v \quad (16)$$

$$P_{\text{connected}}(v) = 0.01863v^3 + 1.898v^2 + 10.5v \quad (17)$$

where v is the linear speed of the bike in m/s . From these results, two observations can be made. The first one is that the disconnected case has a negative cubic term which is not physically possible. This term is because we were unable to set all the parameters of the tests constant, as is possible in a lab, and also because the correlation represents an approximation of reality. This issue leads to having a lower required mechanical force at low speeds for the connected axle than for the disconnected axle which is not plausible. Furthermore, it can be observed that between the two equations, the main difference is the order of magnitude between the losses directly proportional to the speed. This is more evident when the difference between the two polynomials is plotted, as seen in Figure 22 below. As the eddy current losses and the iron losses are proportional to the square of the speed, the main difference is attributed to mechanical losses such as the chain's friction and possibly the ball bearing losses. The eddy current losses and the iron losses are negligible in the case of the bike.

We will therefore assume in the following section that the eddy current and iron losses in the motor are negligible, and that the equation above directly provides the mechanical power necessary to drive a bike at a given speed on a flat surface (the gravitational forces will have to be added to this result).

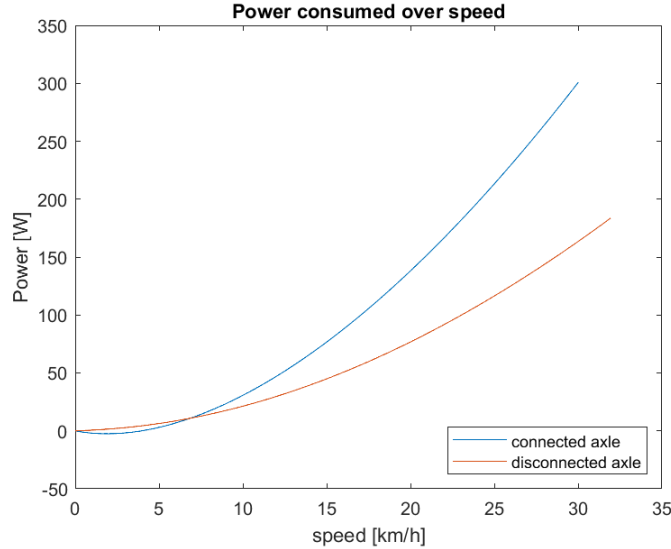


Figure 21: Mechanical losses as a function of speed.

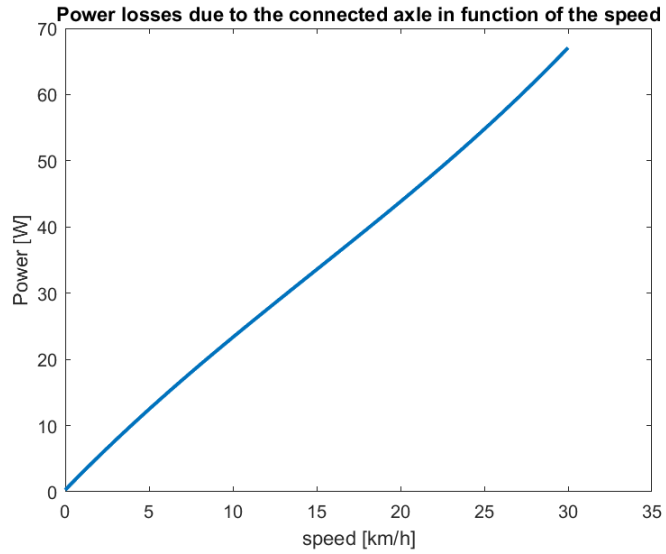


Figure 22: Mechanical losses as a function of speed (connected axle).

2.6.3 Computation of the controller-motor efficiency.

Now that the required mechanical power at constant speed can be computed, the efficiency of the rest of the system, which includes the controller and the motor efficiencies (excluding ball bearing losses as stated in the previous section), can be computed.

To compute this efficiency, we drove the bike at different constant speeds, and also on varying slopes. By doing so, we were able to get an estimation of the efficiency map of this system, or in other words, to study the impact of the bike's speed and the required mechanical force on the efficiency. This test was only performed with the connected axle. When the motor is providing power, the mechanical losses of the chain are present and therefore all the different scenarios are equivalent to the connected, non-regen deceleration scenarios.

The main losses in this system largely come from the motor, and partially from the controller. The map shown in Figure 23 below is to be expected as it shows that the torque and rotational speed of the motor can be translated to a force vs speed map using the gear ratio and the wheel diameter. In theory, our experimental data should follow the global trends of this graph. As the efficiency provided by the supplier is under 80%, the values given in Figure 23 are higher than those expected for the prototype. In addition, the experimental values should only represent the left part of the graph as the nominal speed of the motor will never be reached due to the limitations of the current prototype.

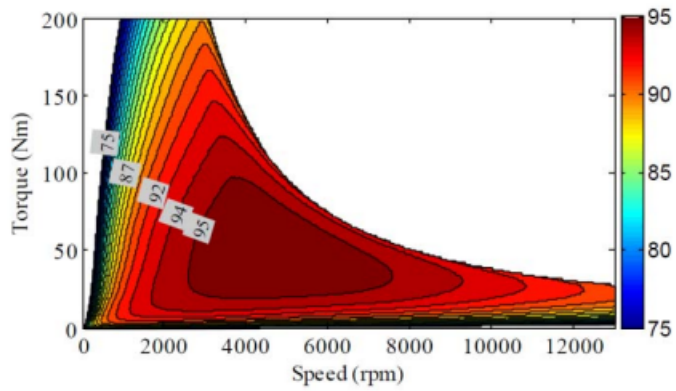


Figure 23: Example of efficiency map of a BLDC motor from [16]

The result of the tests for different speeds on three different slopes, -1° , 0° and 4° can be seen in Figures 24a, 24b and 24c, respectively.

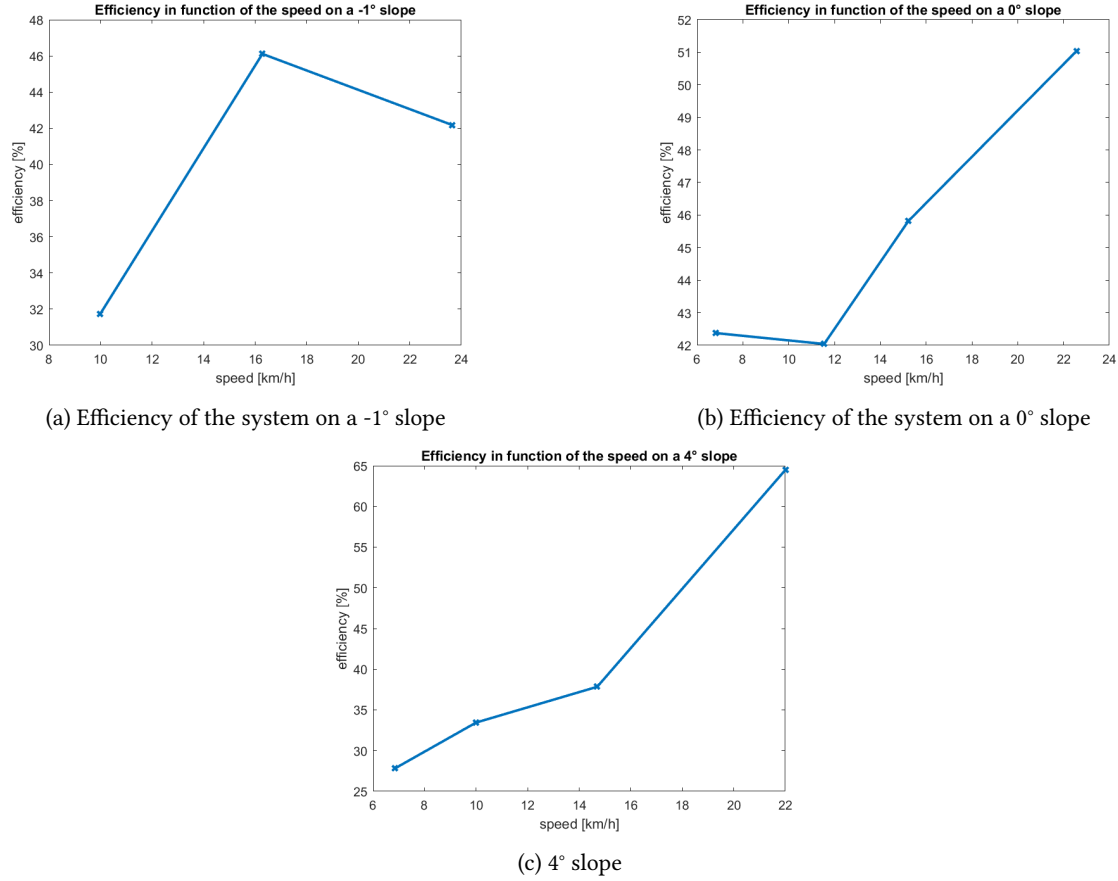


Figure 24: Efficiency of the system over speed on different slopes

From the graphs seen in Figure 24, it can be observed that for the last two graphs, the efficiency increases with speed and is always lower than the nominal efficiency. A 3D plot was created to identify more trends and similarities with the expected efficiency map, shown in Figure 25. Figure 25 shows the distribution of the previous points and their interpolation on a 3D force speed map.

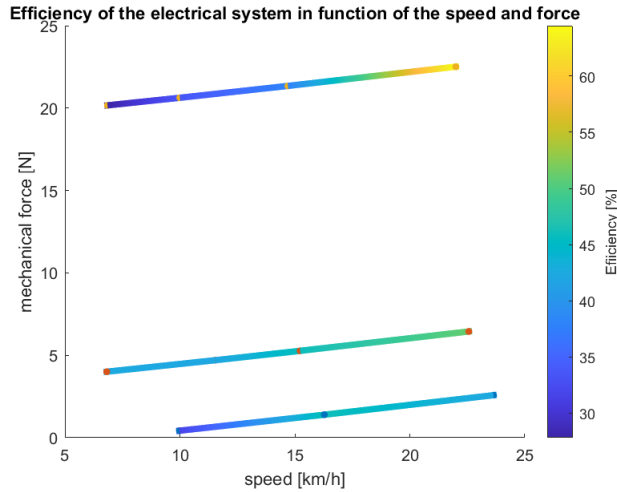


Figure 25: Experimental efficiency map

From Figure 25, the system's efficiency increases with speed for the same amount of mechanical force. Studying the impact of the torque is a bit more complex. At low speeds, the efficiency starts increasing before decreasing with an increase in force. At high speed, the efficiency only increases with the slope. Therefore, the maximum efficiency reached in the tests were at high torque and high speed. It was suspected to be in the low speed, low torque area of the efficiency map of the motor (the area framed in green on Figure 26).

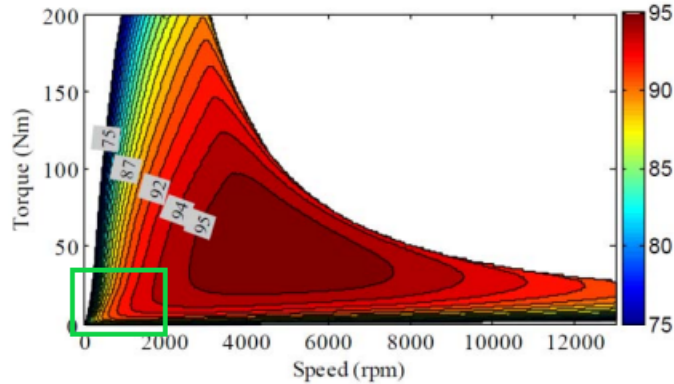


Figure 26: Area of the efficiency map of the experimental tests.

2.6.4 The different tests are made based on the energy consumption

To validate our proof of concept and understand the impact of adding a disconnected axle in an electric car, we need to compare two cases:

- A connected axle with regenerative braking
- A disconnected axle without regenerative braking

Our purpose is to compare the consumed power in each case while taking into account the power that would be regenerated with the regenerative braking system. In doing so, it is possible to determine which solution is consuming the least energy for each scenario.

Therefore, to realize that comparison, it was required to measure and record those energy exchanges. The battery was isolated and over time, we computed the amount of energy that is theoretically flowing out of and into the battery.

In the case of a disconnected axle, the power is only transferred in one direction: from the battery to the motor. The motor can only provide mechanical power and is not able to convert mechanical power into electrical power to transfer to the battery. In the case of the regenerative braking system, the power can flow in two directions: the battery can provide electrical power that is converted by the motor into mechanical power, but also when the bike is decelerating, a part of the mechanical energy is converted by the motor into electricity (therefore becoming a generator) and flowing back into the battery.

To create a comparison, the same scenarios were tested with the two different methods: with the axle that is disconnected and with the regenerative system activated. Then, the total energy transfers were computed, $E_{battery-out}$ and $E_{battery-in}$:

- Calculation of $E_{battery-out}$

To determine the amount of energy that was provided by the battery to the motor, the data gathered by the Arduino board was used. This power can be computed by multiplying the battery's current and voltage. Then, this instantaneous power is integrated over time to compute the total energy provided by the battery during the test.

- Calculation of $E_{battery-in}$

In the case of the regeneration, part of the energy that is lost by the deceleration of the vehicle is transformed into electricity and flows back into the battery. To compute this theoretical energy recovered, the mechanical power lost at each moment due to the regenerative system can be computed: $P_{regen} = F_{regen}v = (m0.1g)v$ and knowing the time between two intervals Δt and the efficiency of that kind of system (around 70% based on [2]), $E_{battery-input}$ can be computed using Equation 18 shown below.

$$E_{battery-input} = \eta_{regen} \Delta t P_{regen} \quad (18)$$

2.6.5 The limitations of the electric bike approach

After having presented the process of building the prototype and characterizing its performance, the similarities and differences between the prototype and an actual EV were analyzed. This allows for a more clear illustration of the values of this comparison along with the biases that it can bring.

The approach used to compare those models was to compare the loss distributions between a GM car and the prototype. Our industry advisor was able to provide the average losses that occur in a car as a function of the speed based on the following parameters: tire force, bearing force, motor and driveline force, brake force, and aerodynamic drag force. Based on the results of section 2.6.2, the basic loss distribution was computed. Assuming the wheel ball bearing losses in the disconnected case as negligible, the $P_{disconnected}$ is related to the tire force and aerodynamic drag force, and the difference between $P_{connected}$ and $P_{disconnected}$ is related to the following components: bearing, motor, and driveline force. In the case of the bike, the brake forces do not exist.

The pie charts shown in Figure 27 below compare this relative distribution of the losses between the bike and a GM car on a flat surface for different speeds: 10, 15 ,and 20 mph. It can be observed that the loss distribution

of the bike losses do not match those of the car. More importantly, the variation of the distribution is higher for the bike than for the car as it has relatively higher losses (nearly three times) than in the case of the car. Moreover, a car is designed to drive at speeds well over 20 MPH and will therefore be optimized for speeds that are unattainable for the bike.

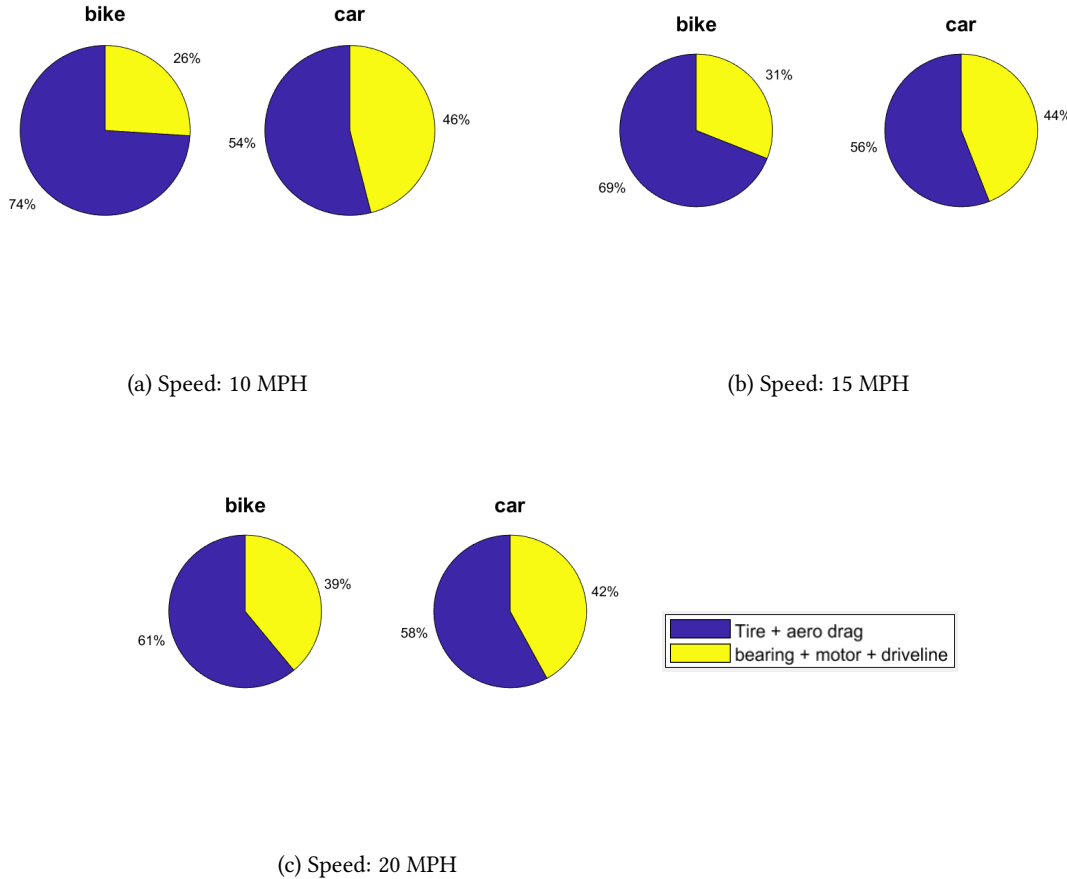


Figure 27: Basic distribution of the losses between the prototype and a GM's car at different speed

Another observation is that the regenerative braking has been set to create a deceleration of 0.1 g in our prototype. This is clearly a source of bias in this study. This modification represents a relative deceleration that is quite small in the case of a car driving at 60 MPH but in the case of our prototype which drives at around 14 mph, this relative difference is more significant. In addition, this prototype does not have the drawback of the weight associated with a real disconnecting axle mechanism. This large relative deceleration at low speeds and the non-existent difference in weight will therefore tend to strongly favor the disconnecting axle.

In conclusion, future test results will have to be analyzed more carefully before being extrapolated or translated to a car. This study is effectively a comparison between an electric bike that is coasting and one with 0.1 g deceleration regen.

2.6.6 The testing methodology for data collection follows realistic driving scenarios

In order to determine optimal energy expenditure between regenerative braking and no regenerative braking instances in driving, four test cases were chosen to be representative of coasting scenarios associated with real driving cases. These scenarios and their associated tests are listed in the table shown below.

Table 2: Realistic Driving Scenarios Conducted

	Driving Scenario	Test Case
Scenario A	Driving with a red light in distance, and the light stays red (Coasting to a stop)	Full throttle for 50 meters, coast for 100 meters.
Scenario B	Driving with a red light in distance, and the light turns green (Coasting to slow down, then accelerating)	Full throttle for 50 meters, coast for 50 meters, and accelerate for 50 meters.
Scenario C	Driving downhill, then flat (Coasting downhill to flat)	Coasting downhill for 50 meters, full throttle for 50 meters.
Scenario D	Driving downhill, then driving uphill again (coasting downhill and accelerating uphill)	Coasting downhill for 50 meters, full throttle for 50 meters.

The test cases were conducted around the UC Berkeley campus at specifically chosen locations that most closely simulated our driving cases. As seen in Figure 28, three different locations were used to complete the testing of our four scenarios. Since scenarios A and B did not require any elevation changes: a flat and straight section of a street was utilized for both test cases. The testing location of scenario C was a downhill street followed by a straight stretch of road at the bottom, while scenario D consisted of a downhill street onto a small strip of flat ground, immediately followed by an uphill portion.



Figure 28: Testing Locations for the Different Scenarios

For each of the scenarios, five trials were performed with regenerative braking and five without regenerative braking to collect consistent and reliable data. Conducting trials with and without regenerative braking en-

abled us to compare results for each of the realistic driving scenarios to examine the potential energy savings of a disconnecting axle.

Table 3: Realistic Driving Scenarios Testing Results

Driving Scenario	Total Energy Used W/O Regenerative Braking (kW)	Total Energy Used W/ Regenerative Braking (kW)
Scenario A	9.67	9.20
Scenario B	11.20	18.12
Scenario C	3.22	5.62
Scenario D	4.57	6.18

The values for test Scenario A show that the average total energy used for the disconnected axle without regeneration case is 9.67 kW, while the average for the total energy used for the connected axle with regeneration is 9.20 kW. The total energy usage for both cases in Scenario A are relatively close with the disconnected axle case having a slightly lower total energy usage. In theory, this similarity is because in both the disconnected axle with no regen case and connected axle with regen case the trials are being conducted on flat ground and accelerated for 50 meters and allowed to coast for 100 meters. The energy gained from the regeneration during the last 100 meters is not that much greater than the momentum the bike gains during its coasting phase after letting off the throttle. However, the data still shows that there is still less energy usage from the regen case because the bike still regenerates more energy during the 100 meter phase with the connected axle than the disconnected axle with the bike coasting.

The values from test Scenario B have an average total energy usage of 11.20 kW for the disconnected axle with no regeneration case. The average total energy usage for the connected axle with regeneration case is 18.12 kW. In scenario B, the total energy usage for the disconnected axle with no regeneration case is a lot lower than the connected axle with regeneration case. Scenario B involves accelerating at full throttle for 50 meters then coasting for 50 meters and accelerating for another 50 meters. The reason the disconnected axle with no regen case is more efficient is because after full throttle acceleration for 50 meters and coasting for 50 meters, the bike is at a much higher speed than the connected axle with regen case, allowing it to accelerate up to speed for the last 50 meters much faster than the regen case. The connected axle with regen setup slows the bike down heavily during the 50 meter coasting phase that it needs a lot more energy to get back up to speed during the last 50 meter acceleration phase that the energy regenerated during the coasting phase is negligible.

The values from test Scenario C have an average total energy usage of 3.22 kW for the disconnected axle with no regeneration case. The average total energy usage for the connected axle with regeneration case is 5.62 kW. In Scenario C, the total energy usage for the disconnected axle with no regeneration is lower than the total energy usage for the connected axle with regeneration case. The disconnected axle with no regeneration case is more efficient because after the initial 50 meter coasting phase the bike was at a much higher speed allowing it to use less energy when accelerating for the last 50 meters on flat ground. In the connected axle with regeneration case, the bike slowed down to a much lower speed during the initial 50 meter coasting phase, so it required a greater amount of energy to accelerate back up to speed during the last 50 meters. Therefore, the energy that was regenerated during the coasting phase was negligible because it required much more energy to accelerate the bike back up to speed than the energy that was regenerated.

The values from test Scenario D have an average total energy usage of 4.57 kW for the disconnected axle with no regeneration case. The average total energy usage for the connected axle with regeneration case is 6.18 kW. In Scenario D, the total energy usage for the disconnected axle with no regeneration case is much lower than the connected axle with regeneration case, meaning it is more efficient. The reason the disconnected

axle with no regeneration case is more efficient is similar to Scenario C, in which the speed the bike gained during the downhill coasting phase is already relatively high, so it takes less energy to accelerate the bike back uphill as compared to the connected axle regeneration setup. On the contrary, the connected axle with regeneration case slows the bike down to such a low speed during the downhill coasting phase that it requires an extreme amount of energy to start up the motor to full throttle and accelerate back uphill, making the energy regenerated negligible.

2.6.7 Study of a daily city commute

After running the tests in the aforementioned specific scenarios, we wanted to expand our potential scenarios by testing a daily city commute of the prototype. With these additional tests, we can gather more practical, real-life data and may notice something different. The choice that we made was to use Vianney's daily commute from his home to Hesse Hall where our capstone lab is located because this course is paved with different interesting cases. It features a straight road with red lights, several uphill sections, and downhill parts when returning home. Thus, this route was a good sample of a driving situation in the city with varying conditions.

Again, the purpose was to compare the case with the disconnected axle and the case with a connected axle and the regenerative braking system activated. As a reminder, the regenerative braking system refers to the servomotors which simulate its effect and the post-test calculations of the energy created.

In the end, we ran four tests for each case and sixteen tests in total. Table 4 shows the average energy consumed by the prototype in the different cases. The tests are quite similar when it comes to the energy consumed, and Table 5 shows that the tests do not vary that much. We have on average a standard deviation equals to 8.05% of the energy consumed, which is decent when we consider the causes of these variations. These variations include the red lights that force us to stop, the pedestrian behaviors, as well as other parameters that we cannot control in an everyday-case test. Despite these uncertainties, we are still going from a point A to a point B and we use the same path, so the energy required to move the bike and its driver along this way is similar. This is the reason why these tests are comparable and why the comparison between the two cases is relevant.

Table 4: Assessment about the overall consumed Energy

	House → Hesse Hall	Hesse Hall → House
Regenerative breaking	150 kJ	133 kJ
Disconnected Axle	103 kJ	99 kJ

Table 5: Standard deviations of the different tests

	House → Hesse Hall	Hesse Hall → House
Regenerative breaking	18 kJ	6.7 kJ
Disconnected Axle	4.4 kJ	10.9 kJ

The main conclusion of this test is that the disconnected axle seems to be more energy-efficient than the regenerative braking system. There is a clear tendency to consume less energy when the prototype is coasting with a low coefficient of friction rather than when we experience a 0.1 g of deceleration and motor losses, even if we recapture some energy.

In Figure 29, one thing that can be noticed is the difference of behavior of the driver between the two cases. Between 25 s and 110 s, we notice that the tester goes at almost constant speed; however, his usage of the throttle is completely different. In the case of the regen, the user keeps a smooth action on the throttle and the input current is quite smooth. In the case of the disconnected axle, the throttle is used intermittently because, as there is less friction, the driver is likely to let the vehicle coast a little before accelerating again. In the case

of the regen, the driver feels the friction due to the 0.1 g deceleration and always keeps the throttle activated to move forward with a reasonable speed. This explains why the vehicle is rarely regenerating electricity and the regen case is clearly less efficient than the coasting. With our prototype, the deceleration is too great to disengage the throttle and allow regenerating energy.

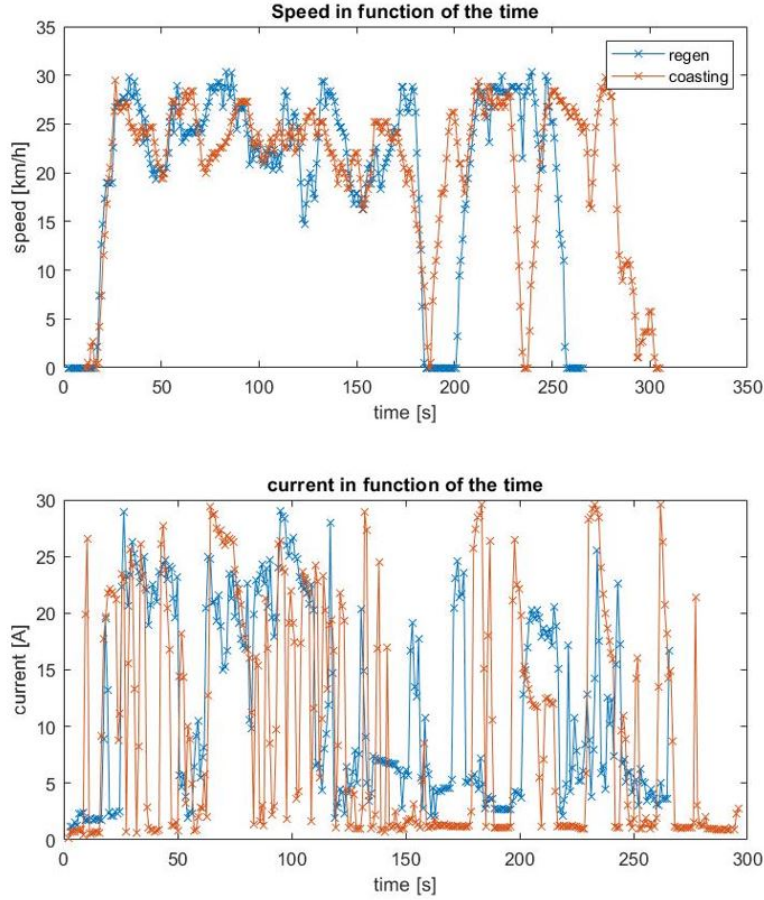


Figure 29: An example of a comparison between regen and coasting from Hesse to Home

Next, we will analyze how much energy could have regenerated if the driver's behavior was similar to the disconnected axle case. We used the data of the test with a disconnected axle and applied the simulation to know how much energy it would have regenerated in Figure 30. We can see that during this time between 25 s and 110 s, there is a lot of energy that would have been regenerated if the driver had not used the throttle. This is not true in the regen case, when the driver have maintained the throttle on during the whole constant-speed time as in Figure 31.

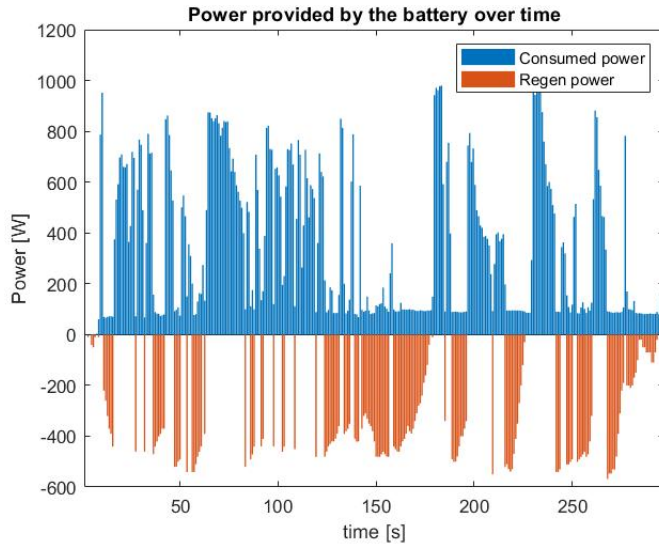


Figure 30: A simulation of a disconnected axle test if it could have regenerated energy

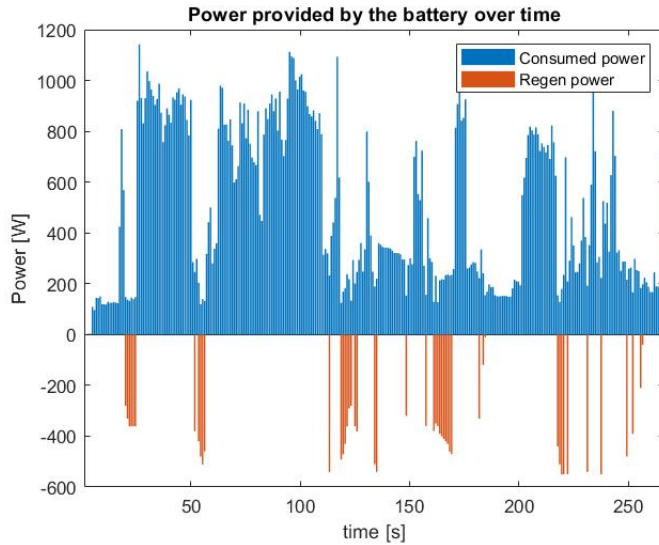


Figure 31: The simulation of Regen in the real case of a Regen test

However, this deceleration is highly different than that of a car. A car is heavier and its speed is usually higher than the speed of our bike. Naturally, the driver will not experience the same deceleration and will be more eager to leave the pedal to let the vehicle coast and charge the battery. Thus, the regenerative braking system is better used in a car which has a larger inertia, rather than on a bike where the rider feels more of the deceleration.

Even if the daily commute tests clearly favors the disconnected axle, we still have to consider that the conclusion will certainly be different with a car because the differences of inertia will have a major impact on

the behavior of the driver. Although the disconnected axle seems promising at first sight, in the context of our study, the speeds and mass of our prototype are factors that we should be aware of when drawing any conclusions because this test only illustrates some differences between a bike and a car.

2.6.8 Impact of the driver behavior on energy consumption

This section of the report aims to outline the conclusions that we made from our different tests. Throughout our tests, we noticed that the driver's behavior had a huge impact on the car's energy consumption. Even within the same case, we noticed a difference of efficiency based on the driver. For instance, the rider may have a sporty driving style with a lot of acceleration to reach maximum speed as soon as possible. This represents a driver who always wants to reach the speed limit despite an oncoming stop sign or red light. In contrast, the driver can also adopt a smooth driving style and try to coast as much as possible to reduce brake usage. In this case, between two stops, the driver will not drive as quickly as possible and will instead reach a moderate speed and then coast to the stop before starting again. That way, a complete stop may be avoided because the red light has more time to turn green while the driver is coasting.

This difference in driving styles is what we wanted to compare in this last section, and to visualize how these extreme behaviors can differ from one another. This is true in the case of the disconnected axle, but also in the regenerative braking case. Therefore, we attempted to drive through four red lights with these two approaches. The first approach is a sporty driving as explained, and the second one is the smooth driving style. The result is given in Figure 32.

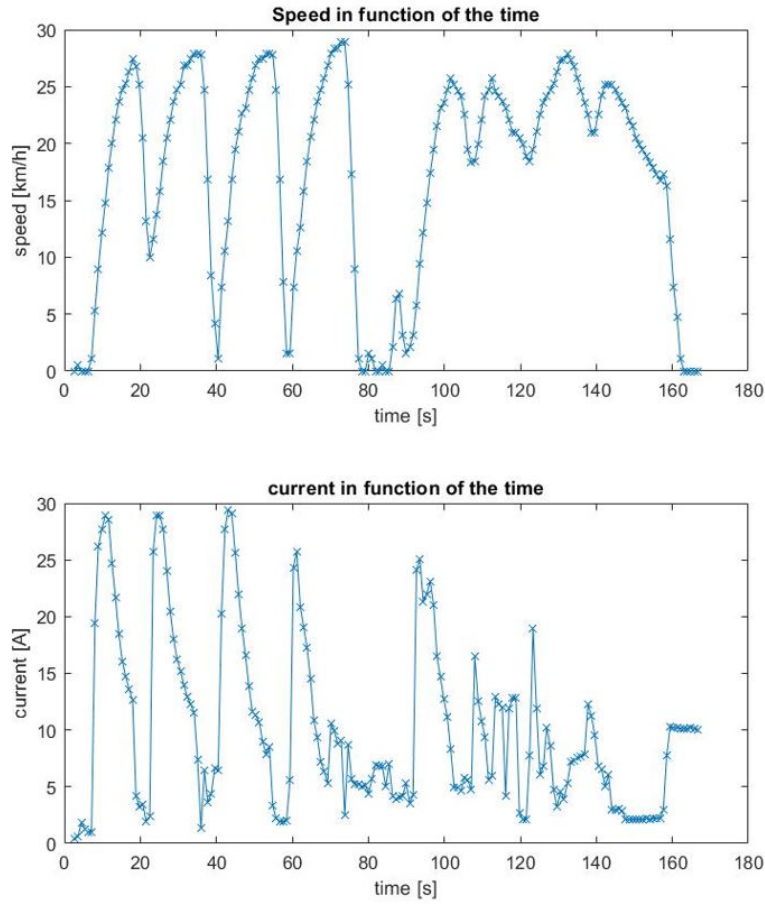


Figure 32: The test of the red lights: a sporty drive VS a smooth drive

We can see that the current used in the first approach is higher than the current used in the second approach. Subsequently, even for the same situation of a flat road with four red lights, the driver's behavior can have a big impact on the energy consumption. Also, in analyzing the energy that could have been produced in the case of using regenerative braking system, like in Figure 33, we see that the energy trends in the same direction. The smoother the drive is and the more constant the speed is, the less energy is used and the more energy is produced from regen. Therefore, the effects are cumulative and amplify the driver's behavior.

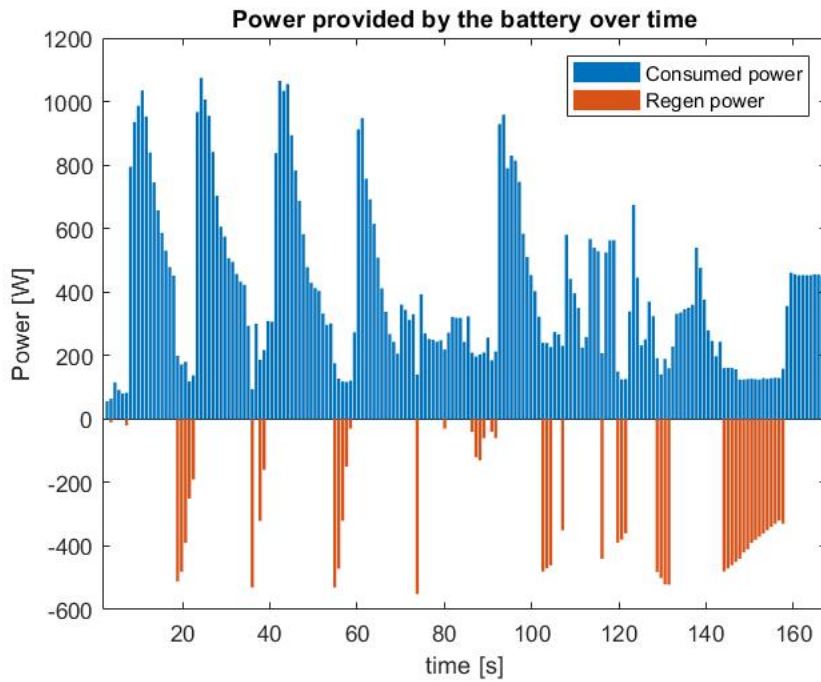


Figure 33: The test of the red lights in terms of regeneration of energy

One question that this short comparison raises is whether we should educate drivers and inform them on adopting an economical driving style or optimizing their vehicle. The best case scenario would be to achieve a combination of the two. Another option is to bypass the behavior of the driver with autonomous vehicles. In this case, the vehicle has to be fully optimized and both disconnected axle and regen could be implemented, with a precise control on when to use which.

3 Conclusion

From the results of the analysis, it was determined that the disconnecting axle case was more efficient than the regenerative braking case in certain scenarios. This advantage can further increase the efficiency of EVs versus gas powered vehicles. However, certain instances during a vehicle's trip allowed for greater energy savings in the regenerative braking case. These instances are very circumstantial, and may offer marginal improvements to the efficiency of an electric vehicle.

Therefore, the adoption of the disconnecting axle technology may contribute energy savings in specific instances. With the use of a disconnecting axle in combination with traditional regenerative braking, and switching between the two based on the driving conditions, EV drivers will be able to save energy during a trip.

As the analysis was conducted using a bicycle prototype, as opposed to a modern commercial vehicle, further research and testing is necessary to determine the comprehensive range of energy a vehicle can preserve with the use of a disconnecting axle. In addition, the instances where energy can be conserved are somewhat obscure and difficult to perceive for average drivers. Therefore, an automated disconnecting axle that detects instances of potential energy savings should be implemented to optimize the efficiency of the technology.

The control of this technology would greatly benefit from the coming innovations in sensing and data collection that are emerging in the EV market, such as LiDAR, GPS, RADAR, ultrasonic, and autonomous vehicle training data. By detecting curves, hills, upcoming lights, and other drivers, a system can be optimized that allows a vehicle to anticipate optimal instances to disconnect the axles or perform regenerative braking. However, the additional weight of a mechanism capable of performing this disconnection may eliminate any efficiency gains made by its inclusion.

Overall, the disconnecting axle technology holds great promise, and could revolutionize the efficiency of EVs in the near future. As the automotive industry moves towards EVs, the growth in electric vehicle efficiency will follow. The disconnecting axle technology is only one solution in a myriad of potential energy efficiency improvements in EVs, and certainly warrants further exploration. Marginal gains in coasting efficiency may outweigh the weight of a disconnecting axle mechanism, but making a final decision on the technology would necessitate more vehicle-specific research. Disconnecting axles in EVs have the potential to further efficiency, and facilitate the world's transition away from fossil fuels in transportation.

4 Appendix

References

- [1] A. Stein. "Electric Vehicle Checkpoint: EV Market May Quadruple by 2030," TheStreet, 18-Nov-2021. [Online]. Available: <https://www.thestreet.com/technology/electric-vehicle-checkpoint-ev-market-may-quadruple-by-2030>. [Accessed: 02-Mar-2022].
- [2] M. Toll. "Regenerative braking: How it works and is it worth it in small evs?," Electrek, 24-Apr-2018. [Online]. Available: <https://electrek.co/2018/04/24/regenerative-braking-how-it-works/>. [Accessed: 27-Apr-2022].
- [3] P. Gupta. "Evaluating Electric Vehicle Market growth across U.S. cities," International Council on Clean Transportation, 20-Dec-2021. [Online]. Available: <https://theicct.org/publication/evaluating-electric-vehicle-market-growth-across-u-s-cities/>. [Accessed: 22-Apr-2022].
- [4] "Electric vehicle sales in California and the U.S." [Online]. Available: https://www.veloz.org/wp-content/uploads/2022/04/Electric-Vehicle-Sales-in-California-and-the-U.S._Final.pdf. [Accessed: 01-May-2022]
- [5] "Electric vehicle market growth & forecast analysis up to 2028," Electric Vehicle Market Growth & Forecast Analysis up to 2028. [Online]. Available: <https://www.fortunebusinessinsights.com/industry-reports/electric-vehicle-market-101678>. [Accessed: 22-Apr-2022].
- [6] 2019 M.B.-A.P.V.-A.A.S.-A.S.G.-A. July 31, "Electric vehicles 101," NRDC, 01-Aug-2019. [Online]. Available: <https://www.nrdc.org/experts/madhur-boloor/electric-vehicles-101#:~:text=Electric%20motors%20makes%20vehicles%20substantially>. [Accessed: 22-Apr-2022].
- [7] ECMA, ECMA-287 Safety of electronic equipment, <https://www.ecma-international.org/publications-and-standards/standards/ecma-287/>,
- [8] Princeton University, Mechanics, https://www.princeton.edu/~maelabs/hpt/mechanics/mecha_55.htm?fbclid=IwAR13pZFE0Cn6fN5wsc-dx4f_IFYHlwtJMrz94acy-rJC4Jd9A31FHzhq3Bk,
- [9] GM Capstone Team, Arduino code for measuring speed, https://github.com/khoan1999/GM-Team/blob/ff06806bd117da0e3eeb22606d7b495fa032e3ec/Arduino_Code.ino
- [10] GM Capstone Team, MATLAB code for analyzing testing data,https://github.com/khoan1999/GM-Team/blob/ff06806bd117da0e3eeb22606d7b495fa032e3ec/MATLAB_Code.m
- [11] Debra, Gyroscopes and Accelerometers on a Chip, <https://www.geekmomprojects.com/gyroscopes-and-accelerometers-on-a-chip/>
- [12] GM Capstone Team, Arduino code for outputting data onto an SD card,https://github.com/khoan1999/GM-Team/blob/ff06806bd117da0e3eeb22606d7b495fa032e3ec/Arduino_Code.ino
- [13] IHPVA, Human power, <http://www.ihpva.org/HPArchive/PDF/hp50-2000.pdf>
- [14] Vukosavic, Slobodan , Electrical Machine, https://search.library.berkeley.edu/discovery/fulldisplay?docid=cdi_uclouvain_repository_oai_dial_uclouvain_be_ebook_52487&context=PC&vid=01UCS_BER:UCB&lang=en&search_scope=DN_and_CI&adaptor=Primo%20Central&tab=Default_UCLibrarySearch&query=any,contains,electrical%20machines%20slobodan&offset=0
- [15] B Guillaume. Very-High-Speed Miniaturized Permanent Magnet Motors: Modeling and Experimental Validation,<https://ieeexplore.ieee.org/ab3079>

- [16] Z. Q. Zhu ,*Quantitative Comparison of Electromagnetic Performance of Electrical Machines for HEVs/EVs*,
<https://ieeexplore.ieee.org/stamp/stamp.jsp?arnumber=7911107>